JOURNAL OF GEOPHYSICAL RESEARCH, VOL. 97, NO. C3, PAGES 3593–3610, MARCH 15, 1992

Drifter Observations of a Cold Filament off Point Arena, California, in July 1988

MARK S. SWENSON AND PEARN P. NIILER

Scripps Institution of Oceanography, La Jolla, California

KENNETH H. BRINK

Woods Hole Oceanographic Institution, Woods Hole, Massachusetts

MARK R. ABBOTT

College of Oceanography, Oregon State University, Corvallis, Oregon

We use the position fixes and temperature readings from 56 Tristar-II mixed-layer drifters, in conjunction with advanced very high resolution radiometer images, to provide a description of the mesoscale variability of the flows associated with cold-water filaments in the California Current system off northern California in July 1988. We find that the northern, offshore temperature front of the filament is convergent and is closely associated with the core of a high-speed (>100 cm/s) jet that has a broader spatial scale than the cold-water filament. Mesoscale features are observed to be related to all developments of the cold-water filament on a variety of time scales (1–30 days). In one well-observed feature, estimates of vertical velocity (w) based on a vorticity budget are −20 m/d over an area of 150 km^2 and are associated with a gain of vorticity. Estimates of w based on a local heat budget following a drifter are about 3 times larger over an area of 60 km^2. These intense downwelling features are also places where horizontal stirring occurs.

1. INTRODUCTION

Although the California Current system has been extensively surveyed since 1949, it was not until the development of satellite-based high-resolution radiometers that the existence of filaments of cold water that extend hundreds of kilometers offshore was appreciated [*Bernstein et al.*, 1977]. It has subsequently been determined that these features are dynamically active [*Davis, 1985; Kosro and Huyer, 1986*] and that there are related structures in biological communities [*Brink*, 1983]. Cold-water filaments appear every year during the upwelling season from May to September when the cold water brought up near the coast provides a source of "dye"; it is not known whether the flows associated with the filaments disappear seasonally along with the "dye." During the height of the upwelling season it is common to see a number of filaments separated by about 60–200 km [*Ikeda and Emery*, 1984] (see also *Flament et al.* [1985] for an image with six filaments). These filaments extend well past the shelf break, so they are part of a larger-scale deep-ocean circulation. The transport in individual jets associated with filaments is large enough [*Kosro and Huyer*, 1986] that the exchange between the shelf and the deep ocean may be dominated by the processes which drive and maintain these structures.

These considerations compelled sufficient interest that a large, interdisciplinary observational effort was organized as the Coastal Transition Zone (CTZ) experiment. An important part of the experimental plan was the deployment of large arrays of water-following drifters seeded at the roots of cold water filaments. The goals of the drifter program were (1) to provide direct, accurate measurements of velocity over the entire spatial extent of the filament, (2) to determine local vorticity dynamics within and around the filament and (3) to infer vertical circulation through conservation principles. In June and July 1988 we released 56 satellite-tracked mixed-layer drifters on the continental shelf and slope near the root of cold-water filaments in the California Current system. These were drogued at 15-m depth and were equipped with four temperature sensors along the drogue tether line. The position fixes from these instruments form the most extensive set of near-surface velocity measurements in the region off the continental shelf of California yet obtained.

In this study we discuss the complex circulations that the drifter trajectories reveal in the coastal transition zone south of Point Arena. Our methodology, including a description of the instruments used, is discussed in section 2. In section 3 we provide a phenomenological description of the transition zone based on drifter overlaid AVHRR images from which other studies may find their context and from which a conceptual picture of the circulation in the transition zone may be formed. We describe the vorticity dynamics and inferred vertical circulation in section 4. We provide separate summaries in the latter two sections. Our main results are as follows: (1) During June and July 1988 there was a filament that extended 350 km offshore in which we measured speeds exceeding 100 cm/s over a distance of 100 km. (2) The temporal development of the filament was strongly influenced by mesoscale variability. (3) The northern, offshore temperature front of the filament was convergent and was closely associated with the core of a jet that has a broader spatial scale than the filament. (4) In one well-

Paper number 91JC02736.
0148-0227/92/91JC-02736$05.00

observed mesoscale feature, estimates of vertical velocity w based on a drifter cluster vorticity budget find rates of -20 m/d over an area of 150 km^2, while estimates of w based on a heat budget find rates about 3 times larger over an area of 60 km^2. (5) It appears that this intensely downwelling feature was additionally a place where horizontal stirring is significant.

2. METHODOLOGY

2.1. *Instruments*

We used the Tristar-II mixed-layer drifter, which has a Dacron sail cloth drogue with three-axis symmetry, tethered by a conducting wire to spherical surface floats [*Niiler et al.*, 1987]. The effective drag area of the drogue is 18.5 m^2, and the drag area of the spherical surface floats and the coated wire tether is 0.240 m^2, which yields a drag area ratio of 77 to 1. Direct measurements of slip of the Tristar-II system with current meters attached to the top and the bottom of the drogue indicate that slip in the direction of wind is proportional to wind speed and inversely proportional to drag area ratio; at a wind speed of 10 m/s a Tristar-II is expected to slip 0.5 cm/s in the direction of the wind. An additional slip in the direction of upper ocean shear is expected to be equal to 0.12 Δv, where Δv is the velocity difference across the 5.5-m vertical extent of the drogue (P. P. Niiler et al., private communication, 1990). During calibration experiments in the California Current we found root-mean-square (rms) velocity differences across 5.5 m of 8.9 cm/s, which would introduce undetermined slips of 1.0 cm/s. The research vessel associated with our field experiment measured a rms wind speed of 12.0 m/s in the vicinity of the drifters. We do not correct for these influences on drifter slip, which we estimate to have a rms value of 1.6 cm/s during this experiment.

The drifters were positioned by Service Argos. The rms accuracy depends on the quality of the satellite fix but is in the range of 150–1000 m per coordinate per fix and is reported along with the fix. This information is used to provide estimates of the standard deviation of each fix that emerges from our processing. Four thermistors were placed at depths of 0, 3.5, 11.8, and 17.4 m on the drifters. These were individually calibrated in the laboratory to within a tenth of a degree Celsius and then potted in epoxy in various ways along the thermistor line. We subsequently discovered that the potting technique introduced random offsets to the thermistor calibrations. Because the sensor at 11.8 m has the least scatter when compared with nearby drifter measurements at the same level and always agrees with at least one other thermistor on the line during early morning when the water column is the least stratified, we adopted it as the reference. The other thermistors were assigned an offset so that wind-mixing events at night provide an isothermal mixed layer to at least 17.4 m. Adjusting the offset at one wind event is sufficient to predict vertically uniform temperature profiles during other events to 0.1°C.

2.2. *Data Processing*

The position data are processed by removing obvious outliers, and nearly contemporaneous positions are averaged subject to the criterion of expected least mean square error using the reported standard deviation of the fixes. This provides a time series wherein the most closely spaced positions are separated by the time of a satellite orbit (about 0.07 days). The data are the linearly interpolated to evenly spaced 3-hour position estimates using a criterion of expected least mean square error under the assumption that the fixes are statistically independent. Velocities are computed by centered differences, which produces 6-hour average velocity sampled every 3 hours along with an explicit estimate of the error of the estimate, which does not account for the "goodness" of the (implicit) model underlying the (linear) interpolation scheme. The temperature data were processed the same way as the positions to provide contemporaneous estimates of position and each of four temperatures for each drifter.

The advanced very high resolution radiometer (AVHRR) data were obtained from the NOAA 9 and NOAA 10 satellites; preliminary processing consisted of (1) geometric correction of the image for viewing angle, (2) conversion of infrared radiance to brightness temperature, and (3) registration of the image to a specified grid. This was carried out by the Scripps Satellite Oceanography Facility (SSOF) using algorithms described by *Young and Fahle* [1981]. The images presented were generated using a linear gray scale with the mean brightness and the contrast manipulated to provide visually pleasing images of the oceanographically relevant brightness temperature gradients, which has the effect of emphasizing mesoscale features. For this set of images, obtained from the SSOF, the coregistration had errors that sometimes exceeded of 10 km. We used unmasked images and made overlays that included the coastline and, without reference to the positions of the drifters or the filaments, subjectively adjusted the overlay so that the coastline fit that seen in the image. We expect that this reduced placement errors to less than 3 km. We reregistered one sequence of images using land references for a study wherein the relative placement of the drifters to the observed temperature gradients was important (Figure 6). This reduced errors to about 1 pixel (1.1 km), at least in regions near the chosen land reference.

One of the drifters (8013A) was equipped with a water sampler and an optical package to study biologically active processes along the drifter track (see *Abbott et al.* [1990] for a description of the instrumentation). The R/V *Thomas Washington* closely followed that drifter from deployment on July 4 to July 10 and provided a platform from which a variety of physical, biological, and chemical measurements were taken. During this time, four additional drifters were deployed within 7 km of the specially instrumented drifter. The dynamics and thermodynamics of the water surrounding this drifter are discussed in detail in section 4. The winds were recorded every 2 hours on board the R/V *Thomas Washington* from June 25 though July 23. During this period the rms wind speed was 12 m/s and the winds were consistently from the northwest, although there was a considerable weakening that began on July 11 (Figure 1). We note that July 1 is day 182 of the 1988 calendar; we will use both methods of reckoning time in this paper.

3. PHENOMENOLOGY OF THE TRANSITION ZONE

In this section we discuss some of the drifter results from the CTZ experiment during 1988 in the form of drifter tracks

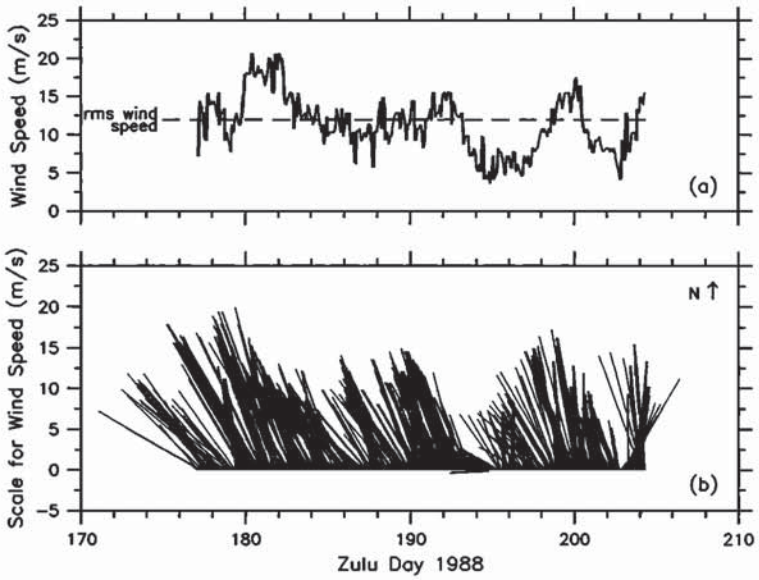

Fig. 1. The winds observed every 2 hours from the R/V *Thomas Washington*. Local time is 7 hours (0.308 days) earlier than Greenwich mean/universal time (Zulu). (*a*) Wind speed. The dashed line represents the rms wind speed over the entire record. (*b*) Wind vectors pointing in the direction from which the wind blows.

overlaying AVHRR images. We find that these descriptive results stand by themselves as important information from which to form a conceptual picture of the circulation in the transition zone. In general, the drifter tracks superimposed on the images are 3 days long and centered at the time of the image, but the tracks may be of shorter duration if the drifter was deployed after the beginning of or failed during the 3-day window. It is important to realize that unlike the drifter tracks, the images are snapshots, so that the choice of the length of the drifter tracks to superimpose involves a compromise between competing factors. Our choice of 3-day tracks for these images emphasizes spatial coverage at the expense of synopticity. That the drifters appear to cross strong thermal gradients is primarily a manifestation of the short time and space scales of the temperature fronts and the nonsynopticity of the tracks and the images.

3.1. *Development of the Transition Zone*

We discuss a sequence of drifter-overlaid images from which we provide an overview of the development of the transition zone from June 27 through July 29 south and west of Point Arena. The drifters were deployed from June 26 until July 15 with distinct arrays on about June 26 (day 178), July 4 (day 186) and July 13 (day 195) (Tables 1 and 2). The June 27 image (Figure 2*a*) shows at least three cold filaments attached to the coastal zone: one emanating north of Point Arena, one emanating west of Point Reyes and one extending south of Point Reyes. The northernmost filament became the object of the comprehensive study. The drifter tracks in Figure 2*a* are from the first deployment of six drifters, and except for one instrument, the tracks are shorter than 3 days (see Table 1). These initial deployments, in the apparent source regions of the filaments near the coast, indicate that there were active offshore flows at the deployment locations of all six drifters. There are three large-scale characteristics of the filament upon which developments we shall focus, although we make additional observations where appropriate. First are the eddies associated with the warm "mushroom" shape that almost reaches the coast near Point Arena. Although the AVHRR signature of these eddies is very weak in Figure 2*a*, it can be brought out by a judicious choice of gray scale map (see inset ii) and is revealed by later drifter tracks. The northern part of the "mushroom" (A) is smaller and cyclonic, whereas the southern part (B) is larger and anticyclonic. The surface signature of these eddies can be traced back to at least June 12, and the intervening images (not shown) suggest that although there is considerable variability in their relative sizes, the anticyclonic eddy is dominant in the sense that it is larger and more stable. Another important feature is the cyclonic eddy at the seaward end of the filament (C), which is very faint in Figure 2*a* and can likewise be brought out by a well-chosen gray scale map (see inset i). The AVHRR images from June 12 onward suggest that a cyclonic eddy, associated with the seaward end of the filament, moved south and west by about 60 km as the filament extended offshore between June 12 and June 27. Finally, we note that a variety of horizontal scales of finer filamentation of cold water are also visible. Water particles, represented by drifter trajectories, pass through the small-scale features as they travel along the filament. We estimate the offshore "phase speed" of the small scale features to be roughly 25 cm/s (e.g. section 4.2.1). They appear to be small-scale instabilities of the broad southward current [*Washburn and Armi*, 1988; Flament et al., 1985] which in the course of their growth are strongly dyed by the cold water on the cyclonic side of the jet and, more faintly, by the warm water on the anticyclonic side farther north.

On July 4 we released 17 drifters directly west in a line of four diamond patterns extending offshore along 39.3°N (Table 1). The drifters began to move rapidly to the south and west; Figure 2*b* is a drifter overlaid image 3 days later. We first direct attention to the coastal region (A). This area, which was a pool of warm water separating the northern two filaments on June 27 (Figure 2*a*), cooled considerably by

TABLE 1. Deployment Data Through July 10

Drifter	Time	Longitude, deg	Latitude, deg	Time	Temperature at 11.8 m
10052	178.149	−123.347	38.200		
10047	178.278	−123.527	38.165		
6190	178.413	−123.625	38.357		
8009	179.005	−124.187	39.112		
10059	179.199	−124.021	39.331		
8002	179.322	−124.300	39.301		
8003	186.526	−123.945	39.342	186.625	9.172
8004	186.546	−124.004	39.388	186.750	9.904
10049	186.556	−124.006	39.342	186.750	9.668
10051	186.566	−124.002	39.297	186.625	9.995
8005	186.583	−124.059	39.344	186.750	10.247
8001	186.600	−124.121	39.388	186.750	10.373
8017A	186.618	−124.118	39.341	187.000	10.650
10057	186.634	−124.118	39.296	186.750	10.224
8008	186.653	−124.175	39.339	186.750	10.247
8006	186.669	−124.237	39.387	186.875	10.381
8013A	186.693	−124.235	39.340	187.000	10.441
10056	186.711	−124.234	39.294	187.250	10.421
6192	186.730	−124.292	39.342	186.875	10.803
10054	186.746	−124.351	39.388	187.000	11.349
8007	186.758	−124.351	39.341	187.000	11.257
10055	186.767	−124.351	39.295	187.000	11.383
10039	186.788	−124.410	39.341	187.000	12.221
10042	188.696	−124.247	38.403		
10040	188.722	−124.325	38.335		
10048	191.260	−125.842	37.776		
10038	192.247	−126.148	37.277		

July 7. A careful inspection of the intervening AVHRR images indicates that the cooling had begun by June 29 (day 181) and was essentially complete by July 4 (day 186). The timing suggests that the cooling was associated with the strong upwelling-favorable wind burst that began on day 180 (Figure 1). The cold water masks the surface temperature signature of the eddies directly south of Point Arena, but their continued existence is demonstrated by the drifter tracks. The small cyclonic eddy is traced out by one of the drifters and the anticyclonic eddy is traced by another, the track of which has been extended by 3 days (dashed line) to make the connection obvious. The southern portion of the anticyclonic eddy circulation appears to be directly involved with the central filament, which was manifest directly west

TABLE 2. Deployment Data for July 13 and 15

Drifter	Time	Longitude, deg	Latitude, deg	Time	Temperature at 11.8 m
10041	195.690	−123.948	39.338	196.000	9.940
10036	195.705	−124.008	39.383	195.875	10.201
10031	195.717	−124.003	39.338	196.000	10.406
10044	195.727	−124.000	39.293	196.000	10.781
10045	195.744	−124.062	39.337	195.875	11.380
6191	195.758	−124.123	39.380	196.000	11.343
10035	195.769	−124.117	39.335	failed	
10033	195.779	−124.115	39.295	196.000	11.381
10034	195.796	−124.177	39.342	196.125	11.742
10053	195.811	−124.236	39.387	196.000	15.580
8013B	195.826	−124.240	39.332	196.000	14.364
10032	195.836	−124.236	39.297	196.000	14.042
8012	195.855	−124.293	39.341	196.000	16.138
10050	195.871	−124.351	39.386	196.125	16.044
8011	195.882	−124.351	39.342	196.000	16.129
10058	195.891	−124.351	39.296	196.000	15.974
8016	195.909	−124.413	39.343	196.000	15.774
8017B	196.002	−124.141	39.117	failed	
8010	197.419	−124.098	38.623	197.500	11.859
8015	197.434	−124.128	38.643	197.625	11.436
8018	197.446	−124.128	38.607	197.625	11.586
10043	197.453	−124.165	38.555	197.625	11.436
10030	197.460	−124.187	38.647	197.625	11.302
10037	197.472	−124.187	38.603	197.625	11.209
10046	197.485	−124.215	38.623	197.625	11.518

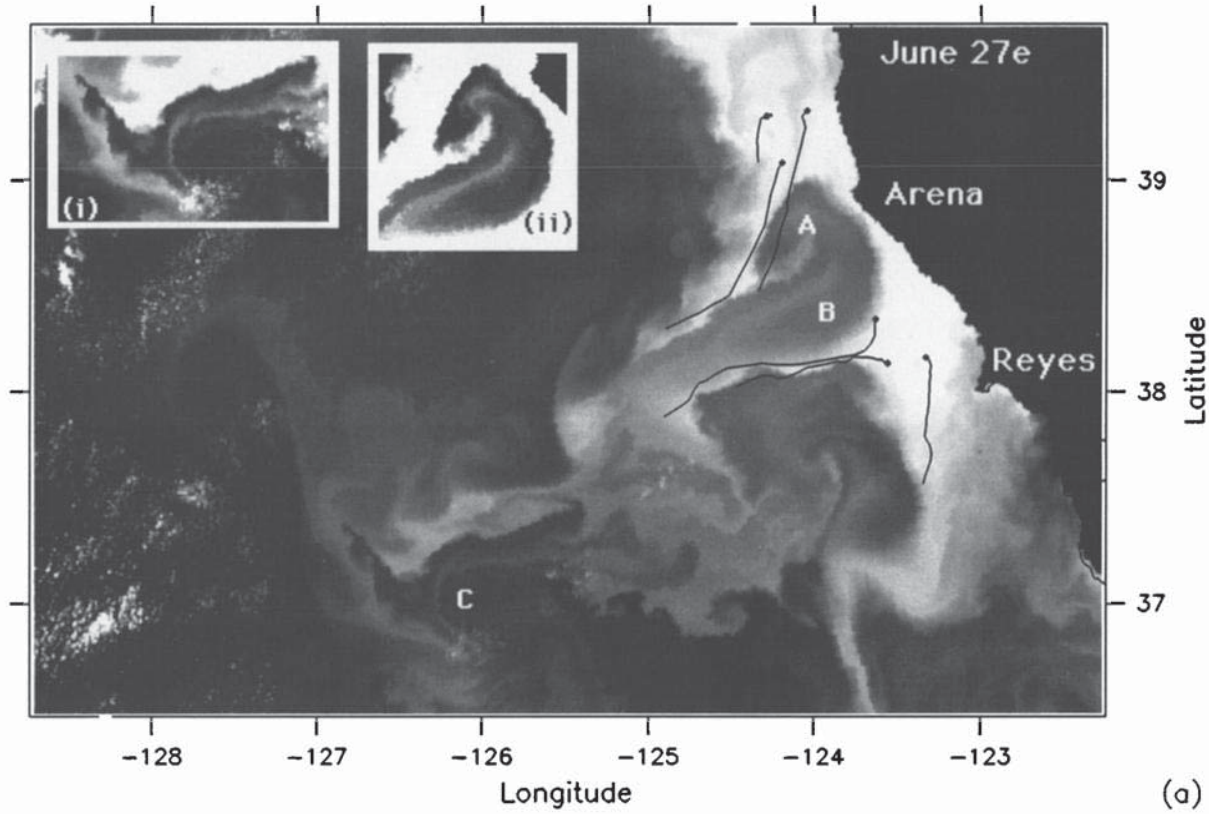

Fig. 2. A sequence of AVHRR images from June 27 to July 28, 1988, superimposed with 3-day drifter tracks centered at the time of the image. Diamonds represent the earliest displayed position fix for each drifter. Some drifters were deployed after the beginning of the 3-day window, so not all tracks are 3 days long (see Tables 1 and 2). The insets that are part of some of the images are sections of the images for which a different gray scale map has been used to emphasize features that would otherwise be faint or masked. Capital Roman letters in the oceanic part of the images are for ease of reference in the text. (*a*) June 27. Inset i corresponds to a section centered on the offshore eddy at C. Inset ii corresponds to a section centered on the warm pool of water near the coast at A and B. (*b*) July 7. One drifter track has been extended by 3 days (dashed line) for emphasis (*c*) July 16. (*d*) July 18. The inset corresponds to a section centered north of A. (*e*) July 28.

of Point Reyes in late June and early July, whereas the western portion of the cyclonic eddy circulation appears directly involved with the northern filament. The seaward eddy is not evident in the AVHRR image, although the convoluted pattern of surface temperature suggests that this may be a region of considerable mesoscale variability. The filamentation of cold water on a variety of horizontal scales has increased during the period of strong winds since June 27 (Figures 1 and 2*b*).

It is also noteworthy that, as seen from the drifter farthest out to sea at about 37°N, 127°W, water particles from north of Point Arena in late June were expelled from the coastal zone to 350 km offshore in 10 days. The drifter that went into the filament south of Point Reyes stayed in that cold-water filament and traveled south. All except this latter drifter ended up in the filament going offshore; as can be seen from these overlays, they tracked the surface expression of the cold water.

On July 13, we repeated the release pattern from July 4 and released an additional cluster of six drifters on the seaward side of the anticyclonic coastal eddy south of Point Arena 2 days later (Table 2). The tracks from these drifters are included in Figure 2*c*. Near the coast, the anticyclonic eddy (A) is well sampled by the drifter tracks with some of the July 13 deployments marking the southward flowing part and the July 15 deployments (Table 2) marking the northward flowing part; this eddy is more than a month old. The smaller cyclonic eddy, wedged between A and the jet on July 7, is not evident. Two cyclonic vortices appear at the seaward end of the filament (B and C).

The image from July 18 (Figure 2*d*) depicts the next development. The drifter tracks reveal that the coastal anticyclonic eddy is severely disrupted by an interaction with an emerging cold-water "squirt" (see inset). Two eddies are still evident at the seaward end of the filament; they appear closer to each other than they did on July 16. A close examination of the drifter tracks suggests strongly that by July 18 these eddies have begun a process by which they merge into one big eddy (Figure 3). The two eddies are clearly shown in Figure 2*c*, the tracks of which correspond closely to those of Figure 3*e*. We believe that the subsequent development (Figure 3) shows that the northeast eddy (feature B in Figure 2*c*), overtakes the southwest eddy (C in Figure 2*c*) and that they merge into a single large eddy by July 24. Notice that there are a number of smaller transient eddies (of both signs, but predominantly cyclonic) in the eastern part of the displayed domain (around 126°W) that may be associated with a transient adjustment process of

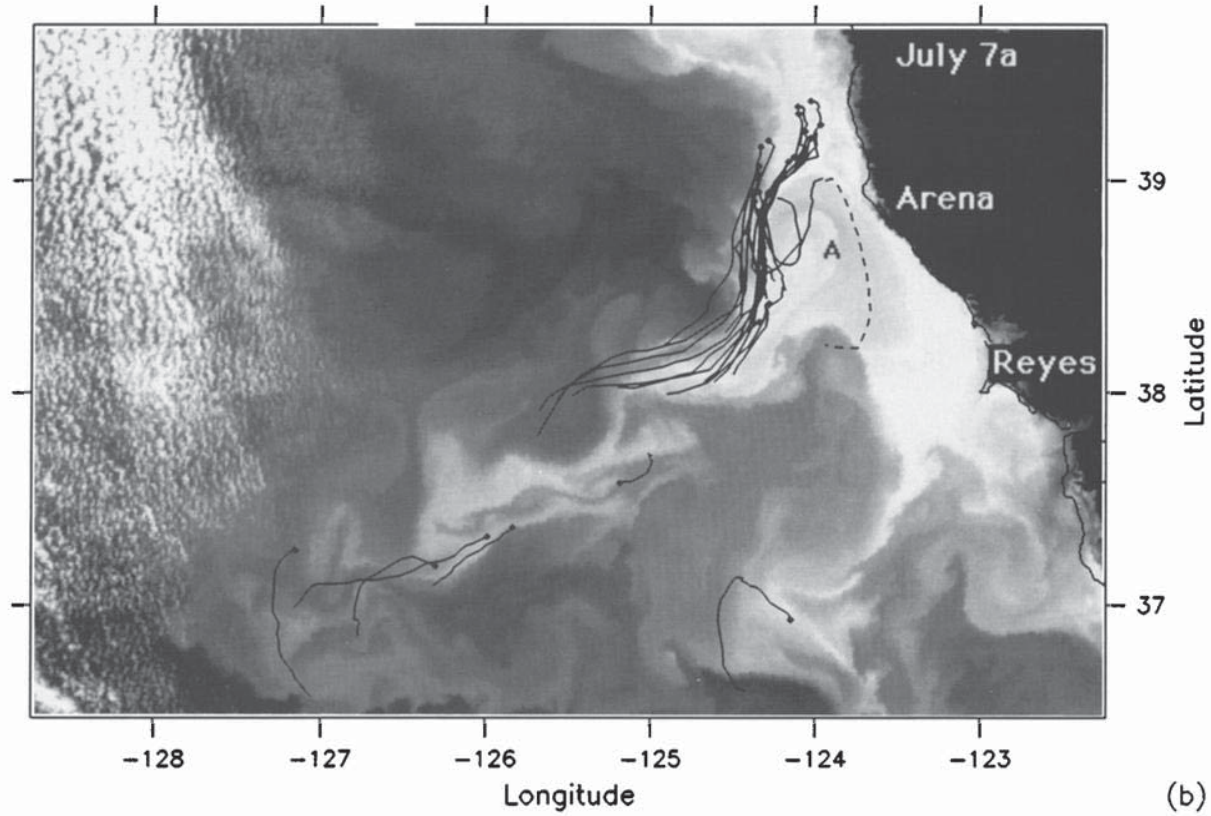

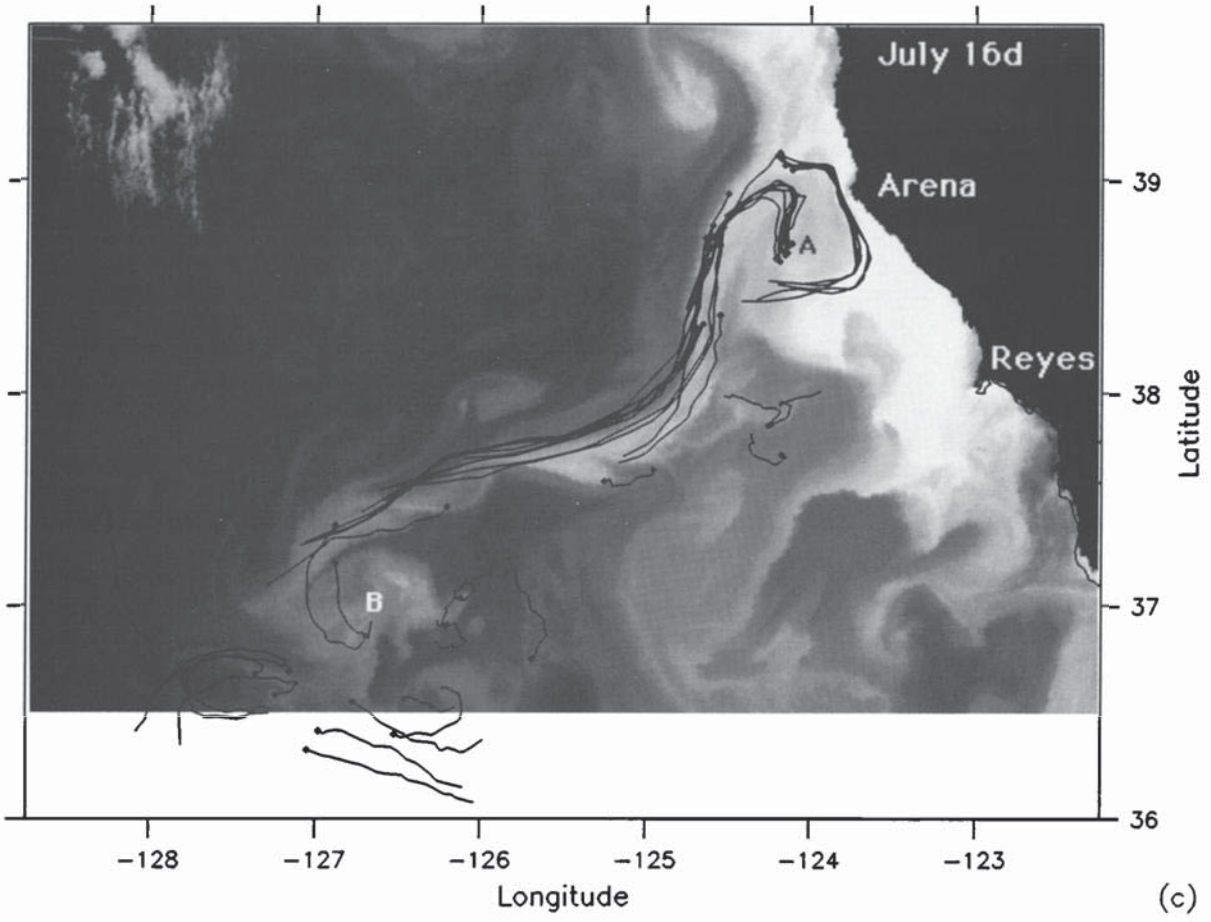

Fig. 2. (continued)

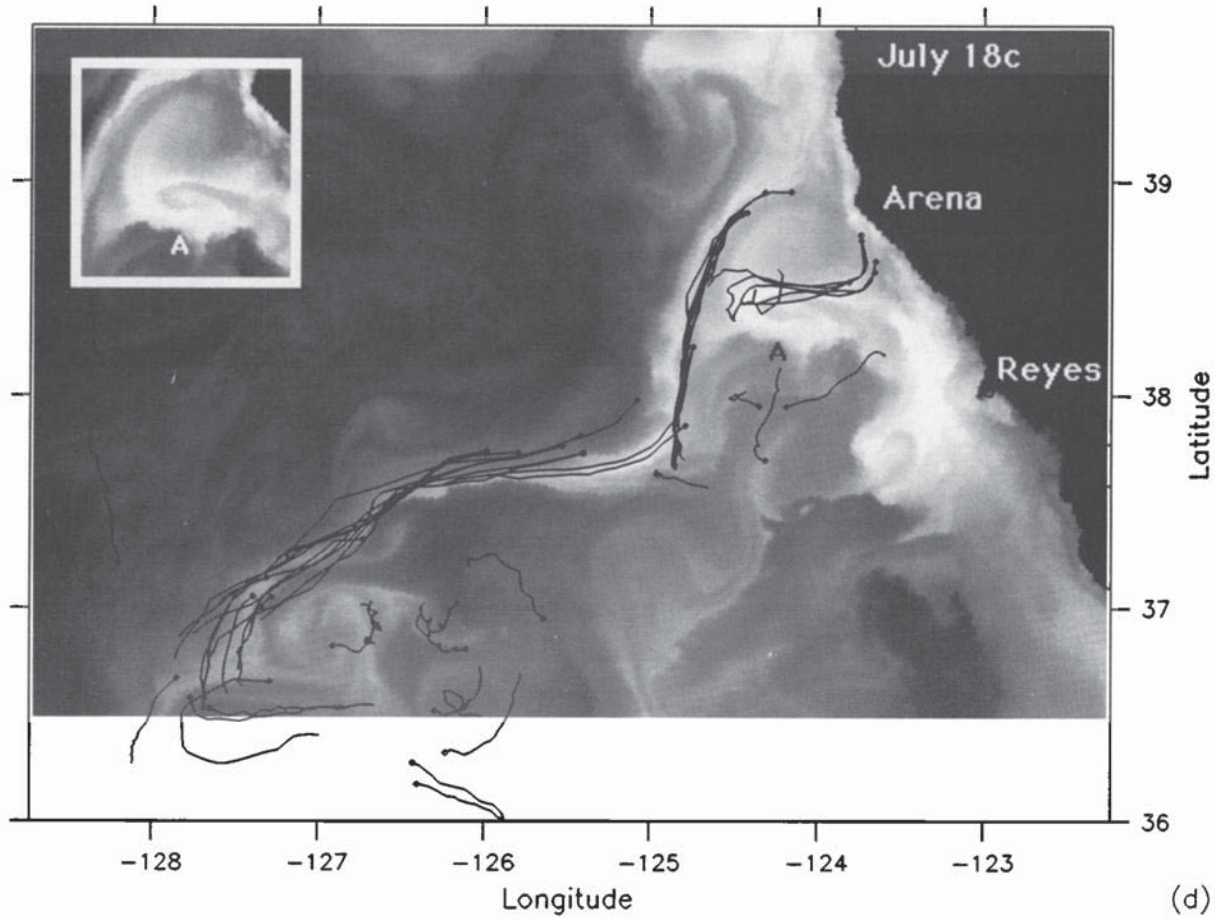

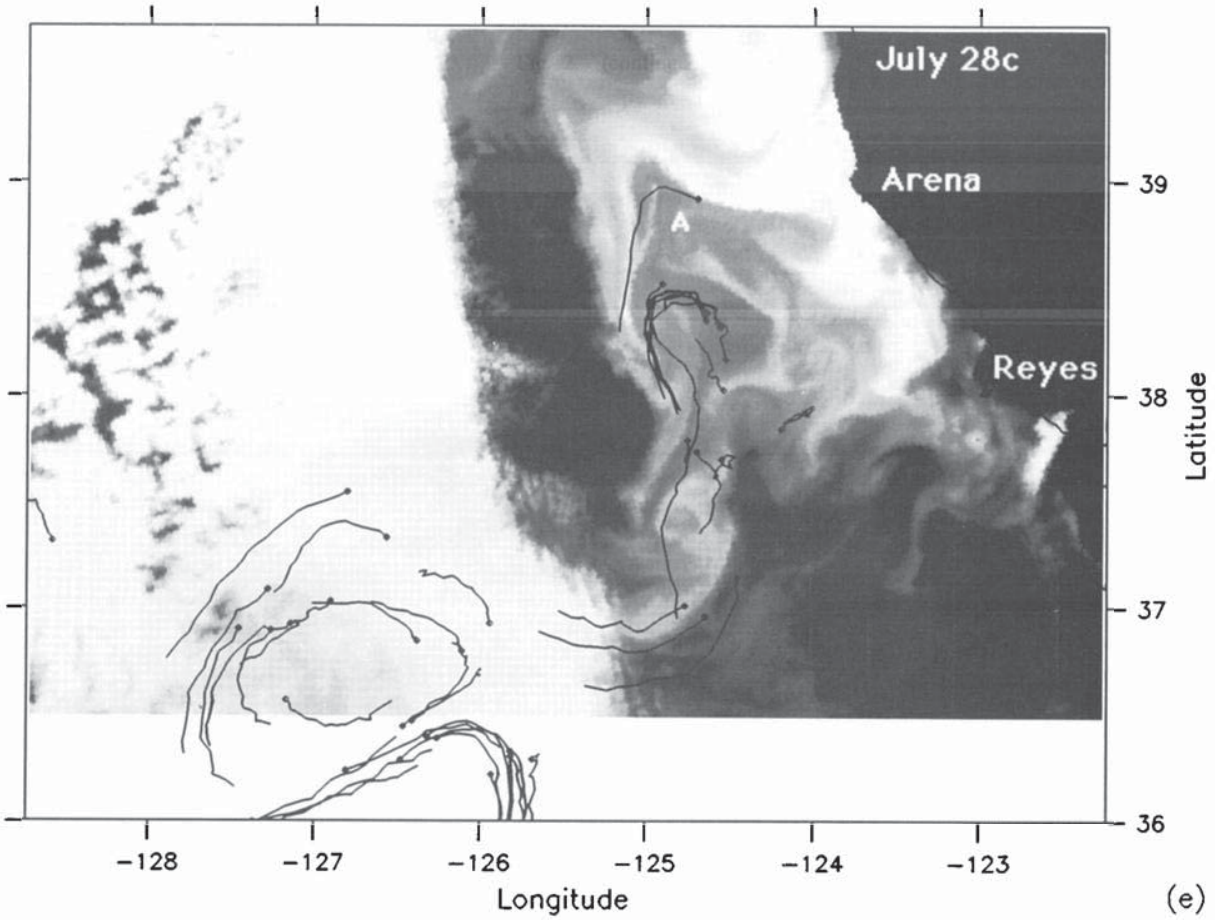

Fig. 2. (continued)

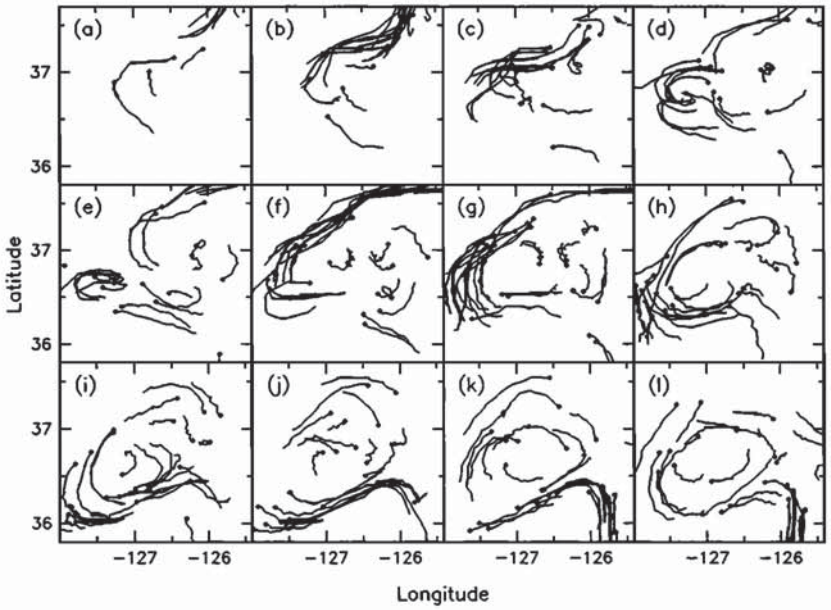

Fig. 3. A sequence of 3-day drifter tracks from 1200 UT, July 8, through 1200 UT July 30, with each panel separated by 2 days. The window of each panel is the same and encompasses the seaward extent of the cold water filament as seen by AVHRR. During this period the region evolved from two or more eddies to one large dominant eddy. (*a*) July 8, (*b*) July 10, (*c*) July 12, (*d*) July 14, (*e*) July 16, (*f*) July 18, (*g*) July 20, (*h*) July 22, (*i*) July 24, (*j*) July 26, (*k*) July 28, (*l*) July 30.

eddy mergers [e.g., *Melander et al.*, 1987]. The large eddy, which is established by July 24, dominates the local flow pattern and is very stable; the drifters continue to circulate within the eddy for another 60 days (not shown [e.g., *Strub et al.*, 1991].

By July 18, nearly all of the small-scale features of the filament had disappeared. From the two main deployments, 26 out of 34 drifters ended up in the rapid flow associated with the filament. Of these, seven exited to its southern, coastal side to become involved in relatively low speed eddying motions, whereas not one drifter exited to the north. It is particularly interesting that all seven that exited to the south were from the July 4 deployment, during which time the filament, as seen in the AVHRR images, had many more small-scale structures than it did later in the month.

July 18 also marks the approximate beginning of another important development in the structure of the filament. It appears that the emergence of the large cyclonic eddy is associated with the collapse of the filament west of 125°W and that a new southward flowing filament was established east of 125°W between about 38°N and 39°N (Figures 2*e* and 4). Until July 18, all of the drifters that reached the first bend in the filament at approximately 38°N, 125°W), turned westward to become involved in the circulation at the seaward end of the filament. Figure 4 shows that the drifters that reach the bend after July 19 (Figure 4*a*) turn east and north to become involved in a cyclonic eddy which releases drifters to go westward only much later (July 27) and considerably to the south (37°N, 125°W) of the original bend (Figure 4*d*). Figure 2*e* shows that this development is accompanied by a similar shift in the cold-water signature on the AVHRR image. Associated with this development is an intrusion of warm water from the south (Figure 2*e*, feature A) which appeared to push the filament northward and offshore of Point Arena. *Huyer et al.* [1991] find that the change in direction of the jet's axis near the center of their grid begins sometime during July 11–18. On the basis of the wind data obtained from nearshore (<30 km offshore) buoys maintained by the National Data Buoy Center off Bodega Bay and Point Arena, they find that the wind reversal began on July 18 and therefore disregard the wind reversal as a possible cause of the jet's reorientation. The wind data obtained from the R/V *Washington* (Figure 1) and the R/V *Wecoma* (not shown; C. Paulson, private communication, 1990), which were taken offshore, show that the wind reversal over the open ocean began around July 11. This suggests that the reorientation of the jet may be related to the relaxation of northwesterly wind which began around July 11.

3.2. *Summary*

To summarize, a detailed examination of the AVHRR images overlaid with drifter tracks yielded the following findings: (1) There were small-scale features associated with the filament that are transitory, decreasing in intensity from early to late July. (2) There was an anticyclonic eddy near the shelf between the major cold filament and the coast south of Point Arena that lasted for at least 30 days (June 12 to July 18). (3) There were two mesoscale cyclonic features at the far offshore end of the filament in mid July which coalesced into a single long-lived cyclonic eddy. (4) There was intrusion of warm water from the south (perhaps associated with a relaxation of the northwesterly winds) that was associated with the deformation of the nearshore filament structure in late July. (5) The growth of the large eddy at the tip of the filament was associated with the breakup of the offshore part of the filament in late July. (6) Drifters that left the filament

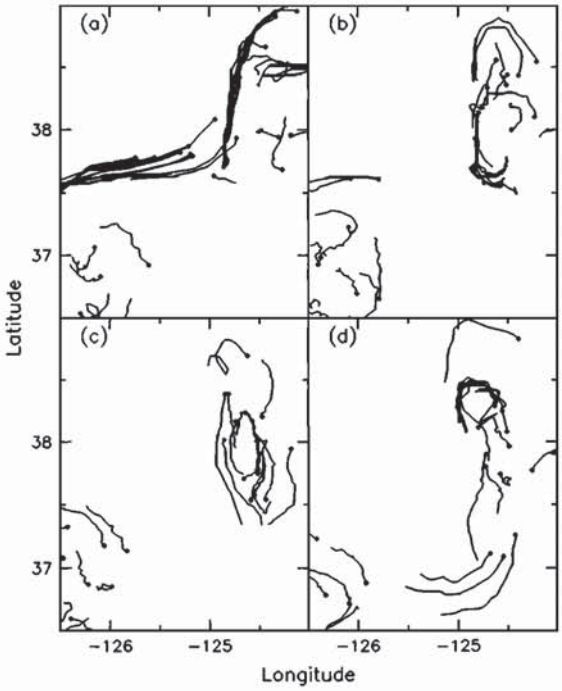

Fig. 4. A sequence of 3-day drifter tracks from 1200 UT, July 18, through 1200 UT, July 27, with each panel separated by 3 days. The window of each panel is the same and encompasses the major bend in the cold filament that existed between the coastal region and the seaward terminus of the filament. This portrays the beginning of a break in the jet structure which had hitherto advected drifters westward at the bend. (*a*) July 18, (*b*) July 21, (*c*) July 24, (*d*) July 27.

did so only to the south and during the time when the small-scale features associated with the filament were numerous.

Our impression from this detailed overlay of drifter and AVHRR images during the month of July is that this cold water filament was related to the mesoscale features, which include the southward flowing jet. For example, we found that two cyclonic swirls of the spatial scale which appear to have been born in the jet produced a long-lived eddy by accretion. This eddy thereby created was associated with the destruction and restructuring of the offshore extent of the filament (and probably the jet). It is also noteworthy that there was a persistent eddy at the location where the jet and filament left the coast; it may have been influential in determining how and where the jet and the filament left the coast. It is probably essential to understand the mutual interaction of the jet and the eddies in order to understand how the filaments are created, maintained, and ultimately destroyed.

Drifters are flotsam, so they tend to aggregate where the 15-m flow is convergent. The cold-water filament entrained nearly all the drifters placed in the vicinity of its root near the coastal zone, which leads us to infer that this flow was generally a converging, sinking pattern. In the next section, we look at a number of clusters of drifters in an effort to understand the vorticity dynamics of some of the events which lead to measurable convergences.

4. Dynamics and Thermodynamics of Mesoscale Events

4.1. *Introduction*

We are interested in the vertical circulation that can be inferred about the flow in and around the cold-water filament. Although drifters follow the horizontal component of flow, we believe that divergence cannot be estimated from this flow directly [*Bryden and Fofonoff*, 1977]. We estimate the vertical velocity from the diagnostics of the vorticity budget following water parcels. This requires accurate estimates of relative vorticity so that its time derivative following the clusters can be calculated. This we obtain by analyzing the relative motions of subjectively chosen clusters of drifters [*Okubo and Ebbesmeyer*, 1976; *Sanderson et al.*, 1988]. Our analysis models the deformation components of the velocity field as constant on the cluster scale. This is reasonable for periods over which the cluster of drifters do not spread appreciably. Our choice of clusters share several characteristics: (1) the elements of the cluster are within 12–15 km of each other, (2) there are four or more drifters per cluster, and (3) the cluster can be followed for a period of 1–5 days. A minimum of three drifters is required to obtain estimates of gradients of velocity, but four or more are needed to provide estimates of the uncertainty of these gradients. In general, this uncertainty is less when more drifters are included in the estimate, but uncertain estimates can still result when the cluster is poorly configured either because the model assumption is invalid on the scale of the chosen cluster or because the cluster assumes a shape that does not allow a good estimate of the gradient in one direction.

The equation for the vertical component of vorticity is

$$\frac{d_H(\zeta+f)}{dt} - (\zeta+f)\frac{\partial w}{\partial z} = -w\frac{\partial \zeta}{\partial z} + \frac{\partial w}{\partial y}\frac{\partial u}{\partial z} - \frac{\partial w}{\partial x}\frac{\partial v}{\partial z} + \frac{1}{\rho_0}\mathbf{k}\cdot\nabla\wedge\frac{\partial \boldsymbol{\tau}}{\partial z} \quad (1)$$

where the relative vorticity is $\zeta = \partial_x v - \partial_y u$, f is the Coriolis parameter, $\mathbf{u} = (u, v, w)$ is the velocity, $d_H/dt = \partial_t + u\partial_x + v\partial_y$, ρ_0 is the density of seawater, and $\partial_z\boldsymbol{\tau}$ is the vertical convergence of the turbulent horizontal stress, which at the surface is equal to the wind stress. Horizontal components of the divergence of turbulent and mean flow Reynolds stresses have been neglected. These are potentially important in a region of rapid horizontal variation on scales smaller than the cluster, but we have no way of estimating their effect. The right-hand side of this equation is small compared with the left basically because the horizontal length scale of the wind is large compared with the horizontal scale imposed by the currents and because the scale depth of the horizontal velocity field is large compared with the mixed-layer depth (see Appendix A). Thus, since w vanishes at the surface, our estimate of w is

$$w(z = -15\text{ m}) \cong (-15\text{ m})\left[(\zeta+f)^{-1}\frac{d_H(\zeta+f)}{dt}\right]_{z=-15\text{ m}} \quad (2)$$

We use a second diagnostic equation based on the heat equation

$$\frac{dT}{dt} = \frac{d_H T}{dt} + w\frac{\partial T}{\partial z} = \frac{1}{c\rho_0}\frac{\partial q}{\partial z} \tag{3}$$

where q is the sum of the turbulent and radiative heat fluxes and $c\rho_0$ is the heat capacity of seawater per unit volume. We can obtain estimates of vertical velocity when there is a vertical temperature gradient $\partial_z T$ by rearranging (3):

$$w \approx \left(\frac{\partial T}{\partial z}\right)^{-1}\left(\frac{1}{c\rho_0}\frac{\partial q}{\partial z} - \frac{d_H T}{dt}\right) \tag{4}$$

We discovered changes of temperature during two events when the vertical temperature gradient was well established and the rate of temperature increase was much larger than could be accounted for by the surface heat flux, which averaged about 180 W m^{-2} (Paulson, private communication, 1990). The net surface heat flux was strongly influenced by the local surface horizontal temperature gradient; the latent heat flux is not much different from zero over the cold water in the filament, whereas it is significant over the warm water. Nonetheless, our estimate of the heating due to the surface heat flux, based on a mixed-layer depth of 30 m, ranges from 0.15°C/d over the warm water to 0.3°C/d over the cold water, whereas we see changes of 2.0°C/d for the events we discuss.

We estimate all time derivatives with centered differences. The vertical derivative in (4) is based on the temperature difference between the two deepest thermistors because they provided the highest quality data, were least affected by the daily surface heating cycle, and were at the depths closest to the drogue center. As was mentioned previously, the estimates of position and velocity have explicit uncertainty estimates associated with them. We can use that information, under the assumption that the estimates are independent, to provide rough estimates of the uncertainty in w from the vorticity budget calculation (see Appendix B). Estimates within 1 standard deviation of zero are not considered different from zero.

4.2. *Results*

4.2.1. *July 4 deployment.* Most of the drifters were released during one of two identical large-scale deployments that were separated by 9 days (July 4 and July 13). The deployments spanned a high-speed southward current associated with a sharp thermal front at the root of the cold filament (Figure 5). The drifters on the offshore side of the array were immediately caught in a strong southward flow and by July 7 the fastest moving drifters had organized into a fairly stable cluster which we refer to as cluster Alpha. An analysis of the motions of this cluster reveals a feature associated with strong downwelling and horizontal mixing.

We show (Figure 6) a sequence of three images with the half-day tracks of the drifters in this cluster superimposed. The feature of primary interest is the pronounced kink or bump in the cold water filament (feature A in Figure 6*a*) which has the appearance of a developing instability. For convenience, we refer to this as the "instability"; we will show that significant downwelling is associated with this

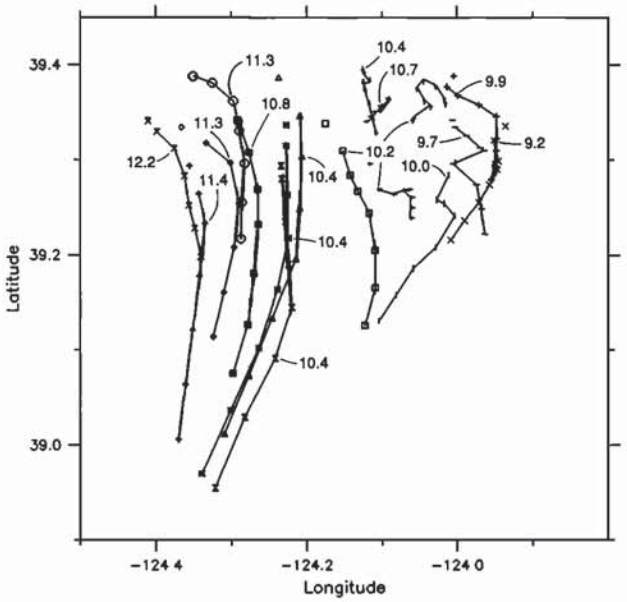

Fig. 5. Deployment positions and evolution through 187.5 UT for the July 4 deployment. The first interpolated temperature reading (in degrees Celsius) at the 11.8-m level associated with each instrument is included (see Table 1). The marks on each track are separated by 3 hours.

feature. Also of interest is the smaller offshore "blob" of cold water at about B in Figure 6*a*. In the first image (Figure 6*a*), the cluster is passing through a warm patch and approaching the cold blob. A day later (Figure 6b) the cold blob has converged and stretched toward the instability, which has moved southwest. The cluster is approaching the instability. The next clear image is 2.5 days later (Figure 6*c*), and we see that the cluster has passed through the instability, which has continued its southwestward movement. The progression of the instability indicates a "phase speed" of about 30 cm/s for 3.5 days, although the average speed of the cluster as it passes through the instability is 75 cm/s.

The simple vorticity budget (equation (2)) suggests that significant changes of vorticity following a cluster will indicate a significant vertical velocity at the depth of the drogue, since w vanishes at the surface. Figure 7 shows the motion of the drifters in the cluster relative to the mean cluster motion at times when the sense of vorticity is easy to see. This visual sense is confirmed (Figure 8) by an analysis of the relative motions. We see that at day 190.0, when the cluster was passing through the instability, the vorticity was increasing sharply. This enables us to estimate w from (2) (Figure 9*b*).

We may obtain an independent interpretation from the heat budget (equation (4)); at the time in question both $d_H T/dt$ and $\partial_z T$ are significantly different from zero (Figure 10). We consider here a subcluster of three which constitutes the center of the full cluster. It appears that the active downwelling region is on a smaller scale than is resolved by the full cluster, but for the vorticity analysis we required a cluster large enough to provide reliable estimates. Our analysis based on the simple heat budget (equation (4)) does not require a cluster at all. We are led to choose a subcluster whose elements exhibit similar behavior and which consti-

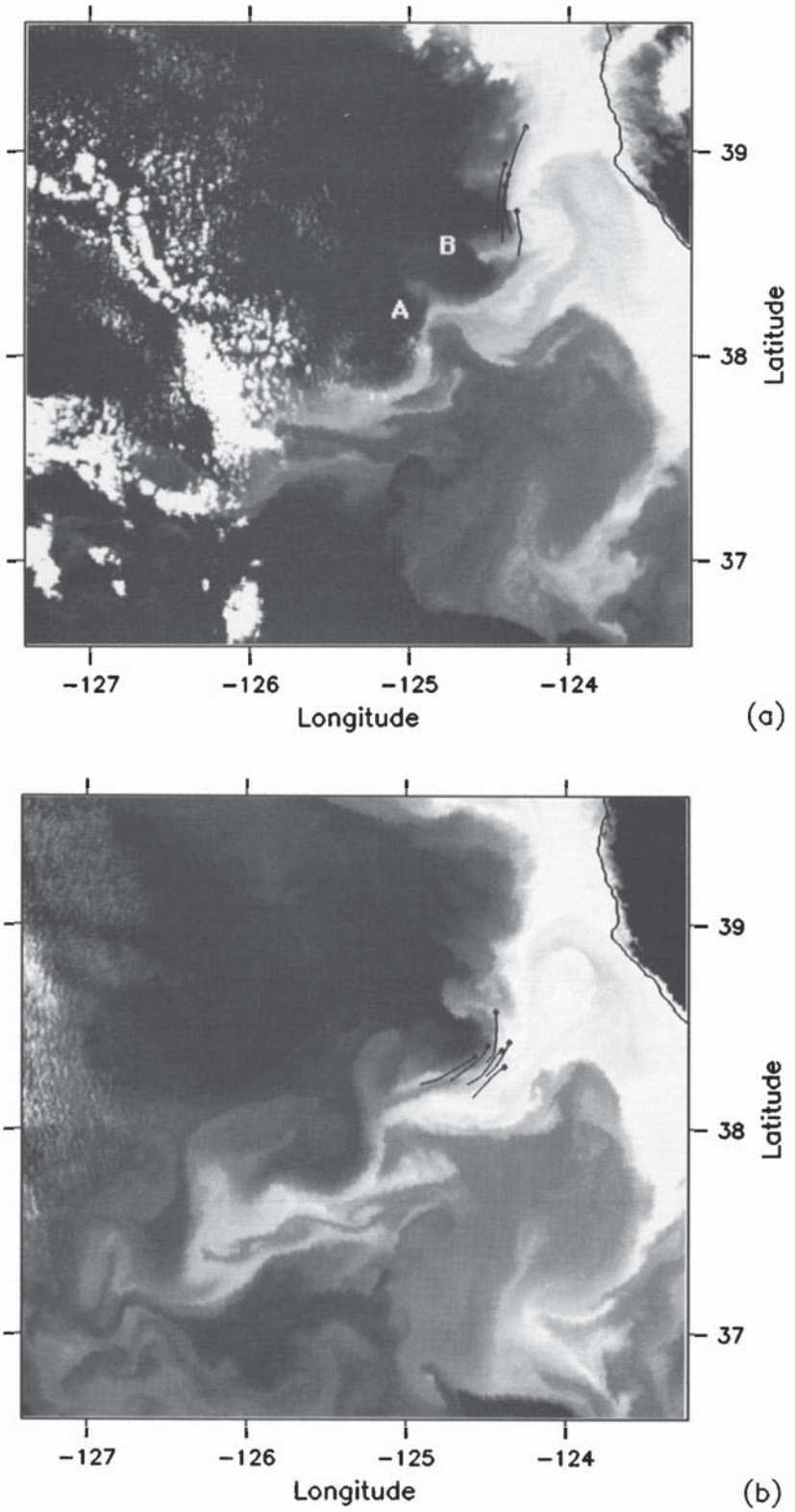

Fig. 6. A sequence of reregistered AVHRR images from July 6 to July 9 superimposed with half-day drifter tracks of drifters in cluster Alpha centered at the time of each image. Diamonds represent the earliest displayed position fix for each drifter. Tracks can start or end within the half-day window, so not all tracks are one-half day long (see Tables 1 and 3). The times of the images are (*a*) July 6 (188.519UT), (*b*) July 7 (189.141 UT), and (*c*) July 9 (191.695 UT).

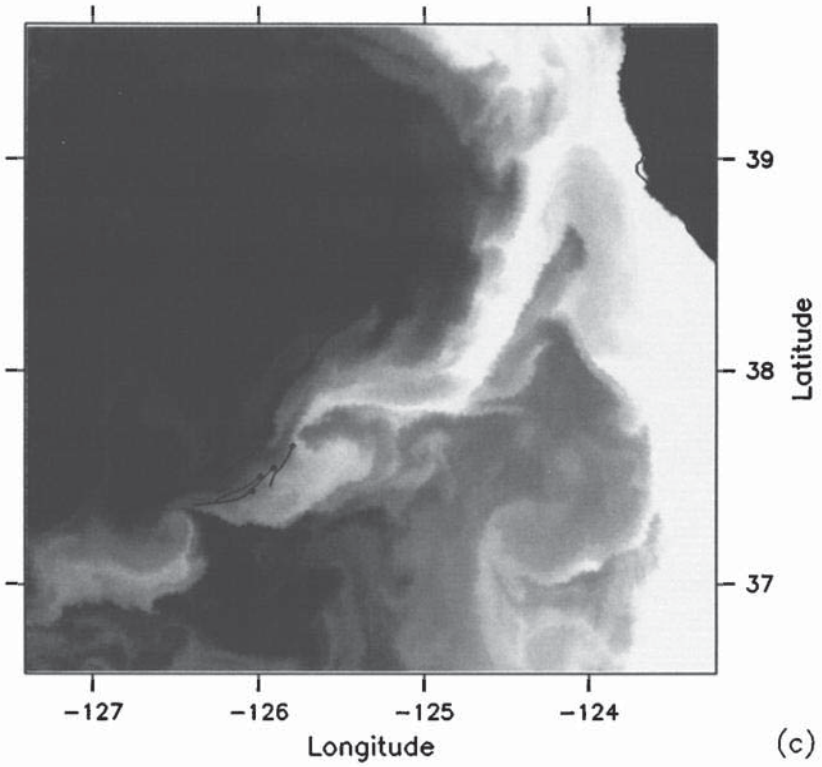

Fig. 6. (continued)

tutes the center of the full cluster considered previously. We neglect the surface flux term in (4) because the temperature increase associated with the passage through the instability is an order of magnitude larger than the net surface heating of about 0.15–0.3°C/d (Figure 10*b*). We also see that this time corresponds to a time of significant stratification (Figure 10*a*) so that an estimate of w from (4) is available (Figure 9*a*). These independent estimates of w display a structure during 187.75 to 190.25 that is similar to the structure of the estimates based on the vorticity budget, except that these heat budget estimates are larger by a factor of 3 (Figure 9). This is not surprising, since the areas of the clusters over which the estimates hold are similarly disparate: the full cluster is about 150 km^2, whereas the subcluster is about 60 km^2. The time that the cluster passed through the instability is unambiguously a time of downwelling.

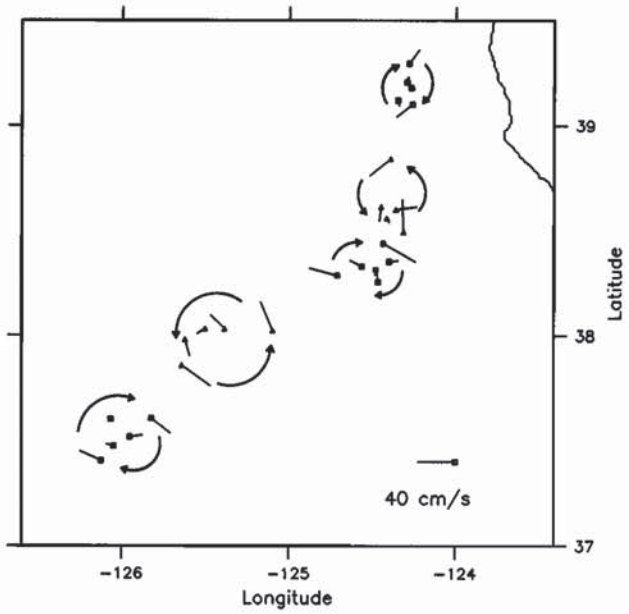

Fig. 7. Velocities relative to the cluster center for cluster Alpha at times when the vorticity is well determined. The sense of rotation is sketched for each snapshot and the associated times from northeast to southwest are 187.250, 188.375, 189.125, 190.500, and 191.625 UT.

Note that unlike the vorticity, the temperature does not rebound after passing through the instability. This suggests a scenario wherein the instability drives a flow across isotherms into warm water as the cold water is subducted. After passing through the instability, the vorticity declines, but the temperature remains high. In the "water parcel" sampled by the cluster, the horizontal stirring occasioned by the instability was followed by an irreversible process which influenced the temperature much more than the vorticity. This could occur near the jet axis (low vorticity gradients) which nearly coincides with the temperature front (see section 4.2.2). Such a scenario is consistent with vertical mixing.

A scenario consistent with our observations of the temperature patterns is that warm water from the north overflows the front, increasing the stratification, with sinking at the drogue level. In this scenario, the slip of the drogue through the water forced by the wind and the vertical shear associated with such overflow would oppose the observed temperature increase, so we do not attribute the observed temperature increase to uncertainties in the water-following characteristics of the drogue system. From observing the interleaving of small-scale cold- and warm-water filaments

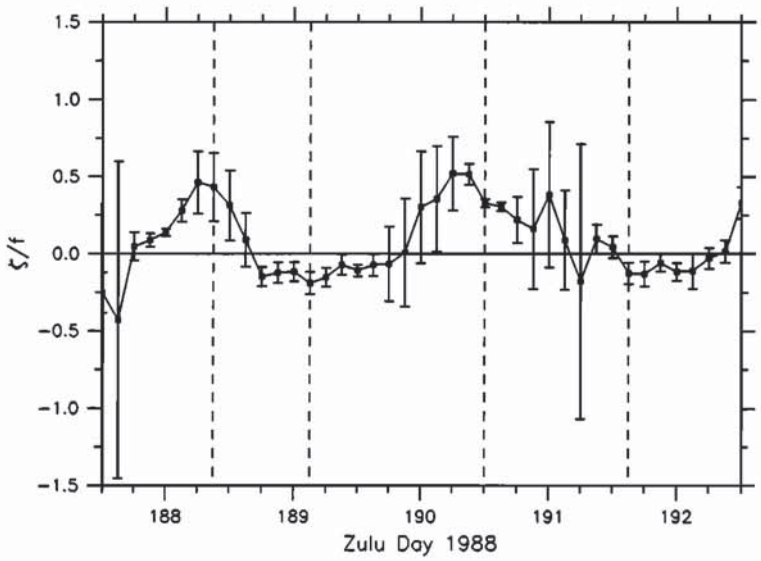

Fig. 8. Evolution of relative vorticity as estimated from the relative motions of cluster Alpha. The error bars represent ±1 standard deviation. The last four times that were sketched in Figure 7 are also shown (dotted lines).

within this instability and from the positive sense of relative rotation that cluster Alpha experienced, we believe that this instability was on the positive vorticity side of the large-scale circulation pattern (the jet). The northern face of the instability was probably at the velocity maximum, as we shall see in the following analysis.

4.2.2. *July 13 deployment.* The development of the second major deployment provides strong evidence that the temperature front nearly coincides with the jet axis and that the jet axis is convergent. As in the first deployment, the deployment array on July 13 spanned the high speed southward jet and an associated sharp temperature front approximately along 39.4°N, 124.2°W, to 39.0°N, 124.3°W (Figure 11). The three fastest moving drifters quickly became separated from the rest and stayed in such close mutual proximity that a vorticity analysis based on their relative motions was not possible. An interesting group, however, did emerge (cluster Gamma), with two drifters on the warm side of the front (drifter identifications, 10050 and 8011) and two on the cold side (6191 and 10034) (Figure 11).

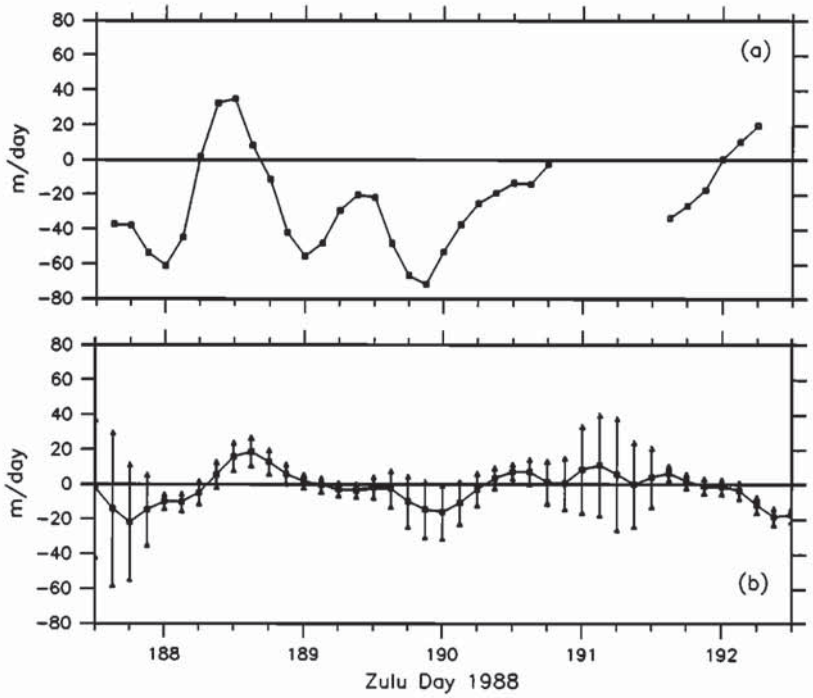

Fig. 9. (*a*) Estimate of vertical velocity obtained from the heat budget of drifters (8013A, 8007, 10055) where significant stratification existed. (*b*) Estimate of vertical velocity obtained from the vorticity budget. Error bars represent ±1 standard deviation.

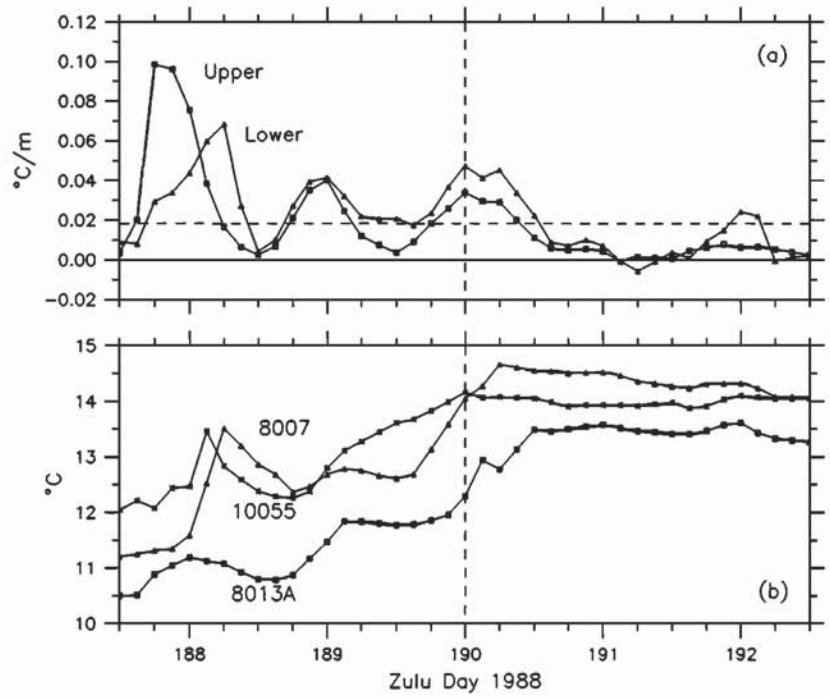

Fig. 10. (*a*) Estimate of average stratification for three drifters from cluster Alpha that experience a significant warming around 190.0 UT. "Upper" represents the stratification between the thermistors at 0 m and 11.8 m, while "lower" represents the stratification between the thermistors at 11.8 m and 17.4 m. The horizontal line at 0.0182 is the stratification resulting from 0.1°C temperature change over 5.5 m and is a measure of uncertainty. The time of maximum downwelling is also shown. (*b*) Temperature history of the three instruments. Triangles, 8007; asterisks, 10055; squares, 8013A.

Observations of cluster Gamma provide considerable evidence supporting our contention that the axis of the jet is convergent. A sequence of AVHRR images with the half-day drifter tracks of this group superimposed are consistent with a scenario wherein the drifters approach the thermal front without crossing it (Figure 12). The temperature histories also support this interpretation (Figure 13) as the temperature contrast across the group declines from about 5.5°C on day 196.0 to about 1.0°C 5 days later. Recall that there is an overall heat flux into the ocean over this time, so that the decline in temperature of the drifters that began in 16°C water is evidence of a vertical circulation. Another piece of evidence for convergence toward the jet axis is provided by a comparison of the state of the group near the time of deployment (196.125) with the state a few days later (199.5) (Figure 14). (The latter time was chosen because the group passed through what appeared to be, based on AVHRR images, a developing mesoscale feature soon thereafter.) In those initial 3.5 days, the cross-jet scale of the group decreased from 16 km to 9 km while the mean speed increased from 38 cm/s to 104 cm/s. We see that the region of convergence, which coincides with the thermal front on the scales we observe, is also a region of strong currents.

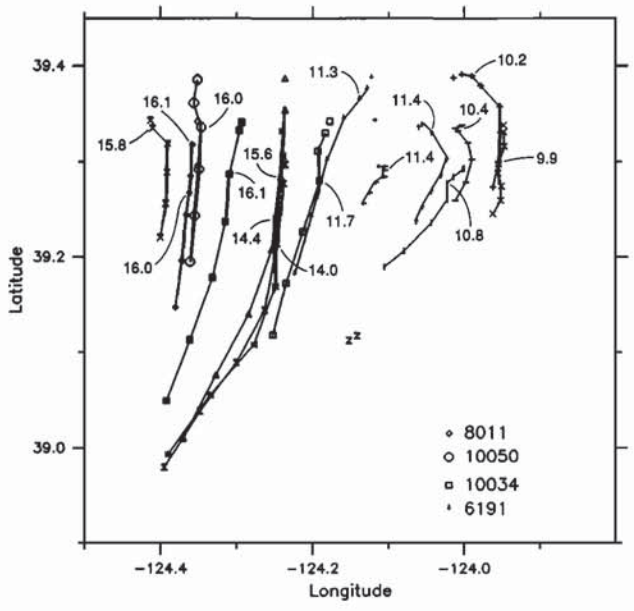

Fig. 11. Deployment positions and evolution through 196.5 UT for the July 13 deployment. The first interpolated temperature reading (in degrees Celsius) at the 11.8-m level associated with each instrument is included (see Table 2). The marks on each track are separated by 3 hours. The members of cluster Gamma are explicitly identified.

The northern two drifters in cluster Gamma were in very weakly stratified water and the southern two in stratified water for the first 2 days (Figure 15). For this situation to occur, there must be mechanical overturning of water on the warm side to keep it vertically mixed in the presence of rather mild winds of the early period of the cluster Gamma trajectory (Figure 1). This suggests that there are significant secondary circulations (vertical and cross-axis) within the flow associated with the filament to maintain such differences of stratification in the upper 15 m over such short cross-frontal distances (see also *Paduan and Niiler*, [1990]).

Observations of several aspects of the nearshore behavior

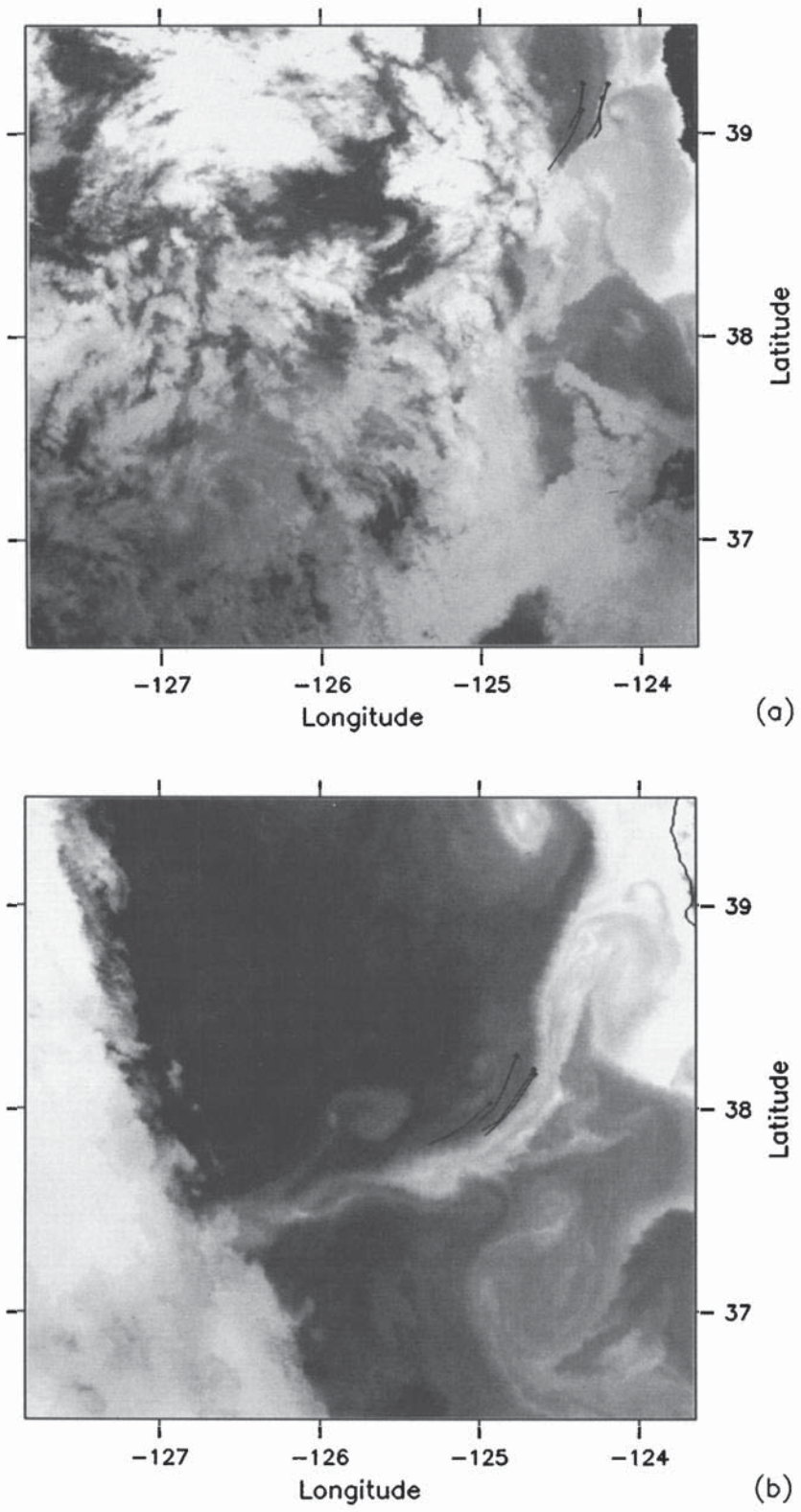

Fig. 12. A sequence of AVHRR images from July 14 to July 17 superimposed with half-day drifter tracks of drifters in cluster Gamma centered at the time of each image. Diamonds represent the earliest displayed position fix for each drifter. Tracks can start or end within the half-day window, so not all tracks are one-half day long (see Tables 2 and 3). The times of the images are (*a*) July 14, (196.668 UT; (*b*) July 16, 198.688 UT; and (*c*) July 17, 199.980 UT.

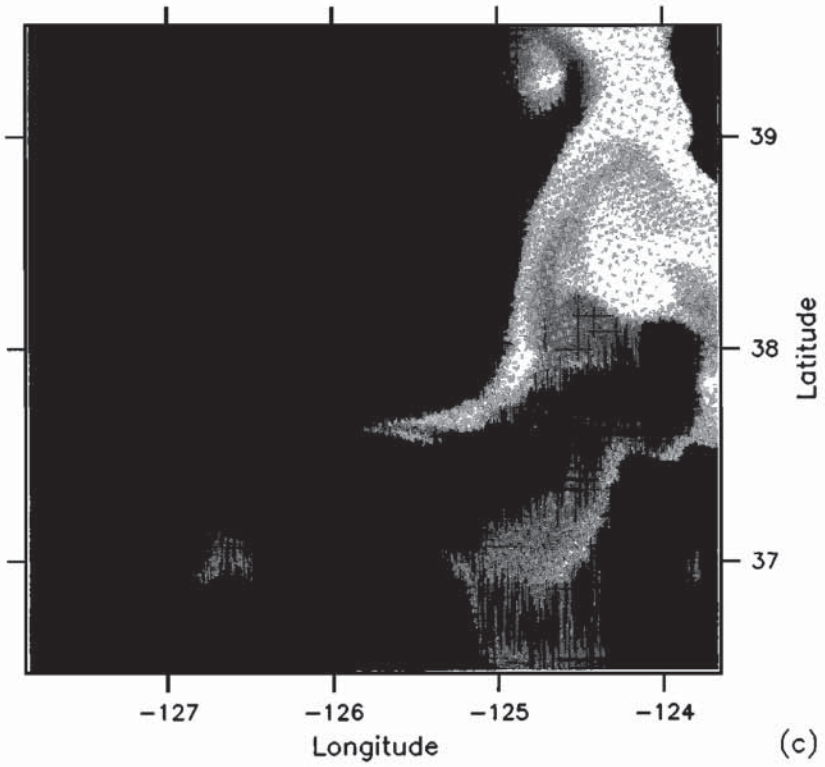

Fig. 12. (continued)

of the deployment array also indicates that the jet axis is a region of convergence. First, Figure 11 provides a visual suggestion that the array is entrained into the high-velocity core of the jet because the drifters that start away from the reign of fastest flow initially move toward the fast-flowing region. Second, we consider a histogram of velocity observations over the first week after deployment for all drifters (Figure 16*a*), and in Figure 16*b* we plot the positions of all high-speed observations (>80 cm/s). Notice that the high speeds are all obtained away from the deployment region, which is consistent with a high-speed core that entrains particles. Finally, estimates of vertical velocity from the positive vorticity side of the jet near the time of deployment substantiate this picture. Using the heat budget with the two cold drifters (6191, 10034), we obtain a downwelling estimate of 80 m/d as the drifters are entrained into the high-speed core. In order to obtain an estimate from the vorticity budget, we consider a cluster that contains the two cold

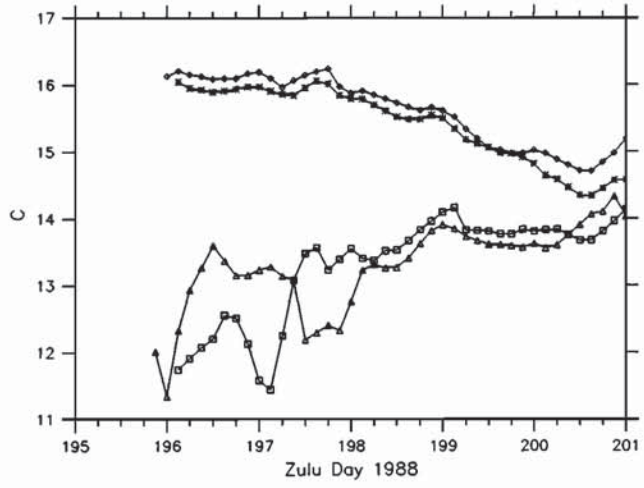

Fig. 13. Evolution of temperature (in degrees Celsius) at 11.8 m for all drifters in cluster Gamma.

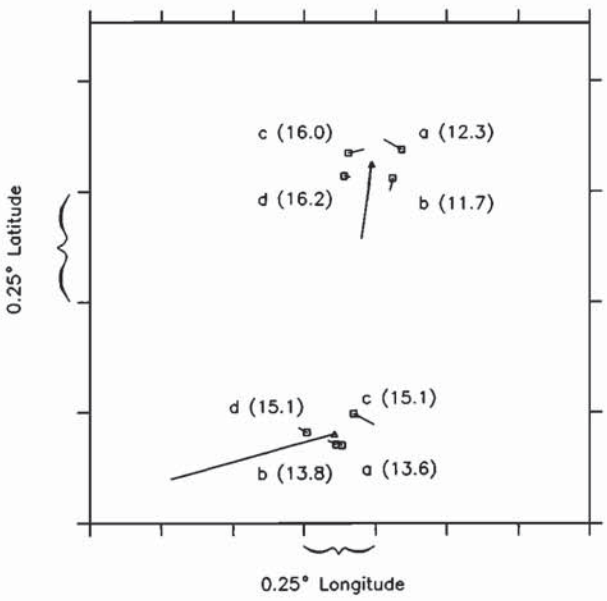

Fig. 14. Mean cluster velocity (triangles) and velocities relative to mean (squares) for cluster Gamma at beginning and end of seaward evolution. The temperature reading associated with each drifter is included: a, 6192; b, 10034; c, 10050; d, 8011.

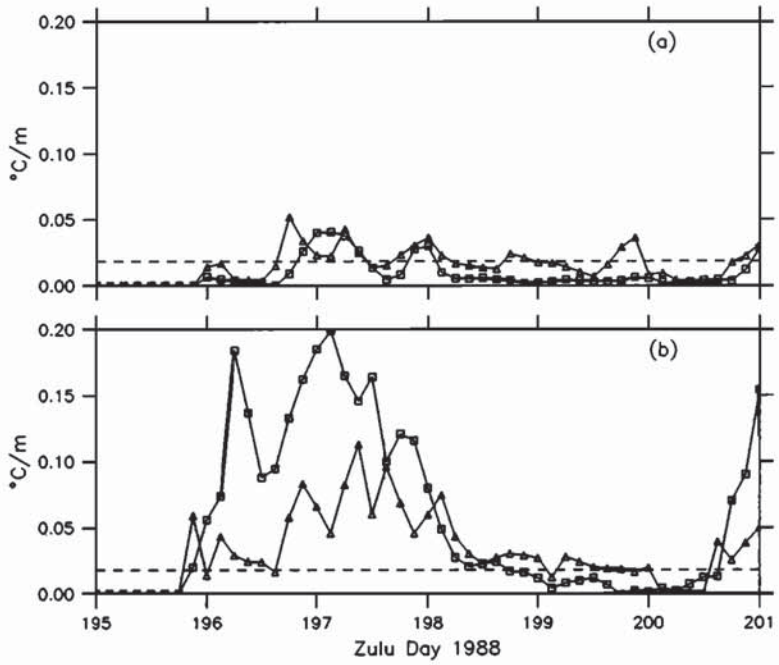

Fig. 15. Stratification history of drifters in cluster Gamma, based on the difference between the thermistors at 0 m and 11.8 m (squares) and based on the difference between the thermistors at 11.8 m and 17.4 m (triangles). (*a*) Warm side, (*b*) Cold side.

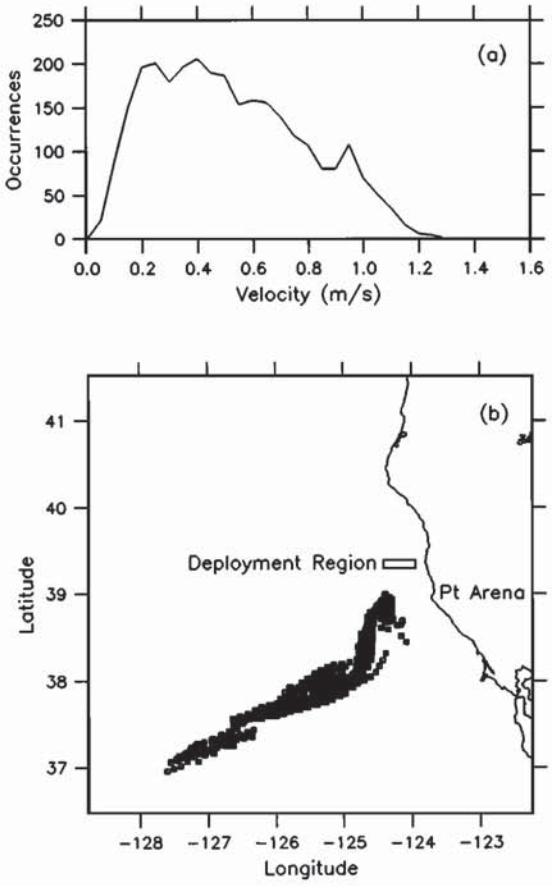

Fig. 16. (*a*) Histogram of all 6-hour average speed estimates sampled every 3 hours for all drifters for the first week following their deployment. Bin size is 5 cm/s. (*b*) Positions of drifters for which the speed estimate is greater than or equal to 80 cm/s.

drifters along with two other drifters situated near the jet axis and obtain $w \approx -20$ m/d. Although these observations are indicative rather than conclusive, they each imply that the high-speed core of the jet is convergent near shore.

Taken together, the evidence from the second large-scale deployment clearly indicates that the jet axis is convergent and nearly coincides with a strong thermal front.

4.3. *Summary and Discussion*

We find that the northern, offshore temperature front is convergent and is closely associated with the core of a jet that has a broader spatial scale than the filament. In one well-observed feature (the "instability"), we find downwelling rates of 20 m/d over a scale of 150 km^2 and 60 m/d over a scale of 60 km^2. The net effect of the instability is an increase in temperature where the vorticity recovered after passing through the "instability" but the temperature did not. We suggest that this arises from a vertical mixing where tempera-

TABLE 3. Composition of Clusters

Cluster	Drifter	Notes
Alpha	8013A	recovered 192.751Z
	6192	
	10054	last fix at 189.586Z
	8007	
	10055	
	10040	judged to leave cluster at 191.0Z
	10048	
	10038	
Gamma	6191	
	10034	
	10050	
	8011	

ture gradients are high due to advection and convergence and momentum gradients are low, i.e., near the axis of the jet.

Typically, there is a temperature difference of 2.0° –2.5°C between the deployment region and the offshore part of the filament in AVHRR images. Although the vertical temperature gradient at the 15-m level is too much influenced by the local vagaries of air-sea interaction to provide a consistent and reliable estimate of vertical velocity, the cyclical nature of the upwelling and downwelling revealed by the analysis of cluster Alpha suggests that there is no net gain of vorticity which would amount to a gradual sinking of the entire filament. A substantial part of the observed temperature difference may be accounted for by differential heating. The heat flux data (Paulson, private communication, 1990) indicate that the cold water of the filament is preferentially heated by about 0.15°C/d compared with the warmer surrounding water. Therefore the jet's surface temperature signal is reduced by bout 1.5°C in the 10 days it takes a typical water parcel to reach the seaward extent of the jet.

APPENDIX A

We scale the vorticity equation (1) using f to scale the relative vorticity, a horizontal velocity scale $U = 1$ m/s which represents a typical speed in the jet, a vertical velocity scale $W = 10$ m/d which represents a typical vertical velocity in the jet, a horizontal length scale $L = 10$ km which represents the scale of the jet, and an advective time scale $T = L/U$, and the curl of the wind stress is scaled by a typical wind stress $\tau_0 = 0.1$ kg/m/s^2 divided by the horizontal scale of the wind, which we take to be 100 km. The only subtle point that arises is that we need to distinguish between two different depth scales. One is the scale of the mixed layer, which we take to be O(10 m) and is the scale over which the vertical velocity and wind stress vary over their full range. The other is the scale depth of the horizontal velocity field which we take as O(100 m), in keeping with observations [*Huyer et al.*, 1991].

APPENDIX B

The estimate of w is based on a ratio of two statistical quantities x and y. If our estimate of w is denoted z, then $z = x/y$ where $x = \langle x \rangle + \varepsilon$, $y = \langle y \rangle + \delta$, $\langle \varepsilon \rangle = 0$ and $\langle \delta \rangle = 0$. Then

$$z = \frac{\langle x \rangle + \varepsilon}{\langle y \rangle} \left(1 + \frac{\delta}{\langle y \rangle}\right)^{-1} \tag{A1}$$

and, under the assumptions that $|\delta/\langle y \rangle| < 1$, $\langle \varepsilon\delta \rangle = 0$, $\langle \varepsilon\delta^2 \rangle = 0$, $\langle \varepsilon^2\delta \rangle = 0$ and $\langle \varepsilon^2\delta^2 \rangle = \langle \varepsilon^2 \rangle \langle \delta^2 \rangle$, we find the variance of z

$$\langle z^2 \rangle - \langle z \rangle^2 = \frac{\langle \varepsilon^2 \rangle}{\langle y \rangle^2} + \frac{\langle \delta^2 \rangle \langle x \rangle^2 + 3\langle \varepsilon^2 \rangle}{\langle y \rangle^2} + O\left[\left(\frac{\delta}{\langle y \rangle}\right)^3\right] \tag{A2}$$

Acknowledgments. We thank Libe Washburn for providing surface wind measurements and Clayton Paulson for providing measurements of wind from the R/V *Wecoma* and surface heat flux measurements. This work was supported by the Office of Naval Research (ONR) contract N00014-89-J-1241 through the Coastal Sciences section (code 1122CS).

REFERENCES

Abbott, M. R., K. H. Brink, C. R. Booth, D. Blasco, L. A. Codispoti, P. P. Niiler, and S. R. Ramp, Observations of phytoplankton and nutrients from a Lagrangian drifter off northern California, *J. Geophys. Res.*, *95*, 9393–9409, 1990.

Bernstein, R. L., L. Breaker, and R. Whritner, California Current eddy formation: Ship, air and satellite results, *Science*, *195*, 353–359, 1977.

Brink, K. H., The near-surface dynamics of coastal upwelling, *Prog. Oceanogr.*, *12*, 223–257, 1983.

Bryden, H. L., and N. P. Fofonoff, Horizontal divergence and vorticity estimates from velocity and temperature measurements in the MODE region, *J. Phys. Oceanogr.*, *7*, 329–337, 1977.

Davis, R. E., Drifter observations of coastal surface currents during CODE: The method and descriptive view, *J. Geophys. Res.*, *90*, 4741–4755, 1985.

Flament, P., L. Armi, and L. Washburn, The evolving structure of an upwelling filament, *J. Geophys. Res.*, 90, 11,765–11,778, 1985.

Huyer, A., P. M. Kosro, J. Fleischbein, S. R. Ramp, T. Stanton, L. Washburn, F. P. Chavez, T. J. Cowles, S. D. Pierce, and R. L. Smith, Currents and water masses of the coastal transition zone off northern California, June to August 1988, *J. Geophys. Res.*, *96*, 14,809–14,831, 1991.

Kosro, P. M., and A. Huyer, CTD and velocity surveys of seaward jets off northern California, July 1981 and 1982, *J. Geophys. Res.*, 91, 7680–7690, 1986.

Ikeda, M., and W. J. Emery, Satellite observations and modeling of meanders in the California Current system off Oregon and northern California, *J. Phys. Oceanogr.*, 14, 1434–1450, 1984.

Melander, M. V., N. J. Zabusky, and J. C. McWilliams, Asymmetric vortex merger in two dimensions: Which vortex is "victorious"?, *Phys. Fluids*, 30, 2610–2612, 1987.

Niiler, P. P., R. E. Davis, and H. J. White, Water-following characteristics of a mixed layer drifter, *Deep Sea Res.*, 34, 1867–1881, 1987.

Okubo, A., and C. C. Ebbesmeyer, Determination of vorticity, divergence and deformation rates from analysis of drogue observations, *Deep Sea Res.*, 23, 349–352, 1976.

Paduan, J. D., and P. P. Niiler, A Lagrangian description of motion in northern California coastal transition filaments, *J. Geophys. Res.*, *95*, 18,095–18,110, 1990.

Sanderson, B. G., B. K. Pal, and A. Goulding, Calculations of unbiased estimates of the magnitude of residual velocities from a small number of drogue trajectories, *J. Geophys. Res.*, 93, 8161–8162, 1988.

Strub, P. T., et al., The nature of the cold filaments in the California Current system, *J. Geophys. Res.*, 96, 14,743–14,768, 1991.

Washburn, L., and L. Armi, Observations of frontal instabilities on an upwelling filament, *J. Phys. Oceanogr.*, 18, 1075–1092, 1988.

Young, T. L., and J. H. Fahle, User's manual for preliminary satellite image processing: Extraction, calibration and location, *SIO Ref. 81-36*, Scripps Inst. of Oceanogr., La Jolla, Calif., 1981.

M. R. Abbott, College of Oceanography, Oregon State University, Corvallis, OR 97331.

K. H. Brink, Woods Hole Oceanographic Institution, Woods Hole, MA 02543.

P. P. Niiler and M. S. Swenson, Scripps Institution of Oceanography, 92093.

(Received July 31, 1991;
accepted August 8, 1991.)